Computers and Mathematics with Applications 118 (2022) 74–84

Contents lists available at ScienceDirect

Computers and Mathematics with Applications

www.elsevier.com/locate/camwa

Kalman filter and classical Preisach hysteresis model applied to the state of charge battery estimation

P. Venegas [a], D. Gómez [c,*], M. Arrinda [b], M. Oyarbide [b], H. Macicior [b], A. Bermúdez [c]

[a] GIMNAP, Departamento de Matemática, Universidad del Bío-Bío, Concepción, Chile
[b] CIDETEC Energy Storage, Paseo Miramón 196, 20014 Donostia-San Sebastián, Spain
[c] CITMAga, Department of Applied Mathematics, Universidade de Santiago de Compostela, E-15782 Santiago de Compostela, Spain

ARTICLE INFO

Keywords:
Hysteresis modelling
Preisach model
Extended Kalman filter
State of charge estimation
Lithium-ion battery

ABSTRACT

The goal of this work is first to include a hysteresis model in the classical equivalent circuit model (ECM) for a battery system and then to improve the estimation of the state of charge (SoC) by applying the Extended Kalman Filter (EKF). The hysteretic behavior of the open circuit voltage (OCV) is modelled with the classical Preisach model used for magnetic materials. The construction of the Preisach operator is made by means of the Everett function identified from experimental data which only involve the charging curves of the battery. Thus, a significant reduction in the time necessary to obtain the measurements is achieved. The model is assessed with some laboratory experiments performed on a lithium-ion battery and the results show that with this procedure hysteresis is very well reproduced, even when interior loops are present. In addition, the use of the EKF allows us to eliminate the measurements noise and ensure the accuracy of SoC estimation. The high computational efficiency and precision of the method, joined to the limited computational resources needed for the numerical implementation, make it particularly suitable for real-time embedded battery management system (BMS) applications. In addition, the proposed methodology is well-adapted to any battery type, independently of the SoC-OCV profile of the hysteresis cycle.

1. Introduction

In the last years, battery modelling has brought the interest of a large number of researchers motivated by different industrial goals. In particular, the automotive industry tries to maximize the driving range and fuel economy of hybrid (HEVs) and electric vehicles (EVs) using large battery packs in demanding applications.

On the other hand, recently studies have shown the effectiveness of full electric buses (EBs) in decreasing greenhouse gas emissions in cities. In Europe, as a consequence of the EU 2050 objective of decarbonizing the transport sector, more and more cities are moving to EBs and thus the number of EBs delivered in 2018 increased by 75% compared to previous year. For its part, China has developed national incentive policies to encourage the battery EBs implementation and now it is at the forefront of this market in the world (the 98% of the global e-bus market in 2018) [12,8].

In this context, lithium-iron-phosphate technology (LFP, $LiFePO_4$) seems to be the better option due to its higher safety levels which matters more at large battery sizes, high cycling-life and competitive price, advantages that offset its slow charge rates. Therefore, the research in this field has also increased [28], largely driven by the rapid growth in sales of EBs.

There are a wide range of battery models for application in EVs with different degrees of accuracy and complexity [19] which essentially comprise electrochemical and equivalent circuit models. The first ones try to describe the chemical and physical processes inside the battery by means of a set of coupled highly non-linear partial differential equations with many material parameters. In this way, the relationship between the cell performance, and macroscopic (battery voltage and current) and microscopic (charge concentration) quantities can be established. Nevertheless, these methods are computationally costly and complex and the value of parameters difficult to be determined; hence, they are suitable for the battery design rather than for simulation and real-time implementations. On the other hand, the equivalent circuit models (ECM) are lumped models representing the battery dynamics by means of electrical components such as resistors, capacitors and voltage

* Corresponding author.
E-mail addresses: pvenegas@ubiobio.cl (P. Venegas), mdolores.gomez@usc.es (D. Gómez), marrinda@cidetec.es (M. Arrinda), moyarbide@cidetec.es (M. Oyarbide), hmacicior@cidetec.es (H. Macicior), alfredo.bermudez@usc.es (A. Bermúdez).

https://doi.org/10.1016/j.camwa.2022.05.009
Received 19 October 2021; Accepted 10 May 2022

sources to form a circuit network on a basis of the dynamic characteristics and operating principles of the battery [16]. Each component has simple mathematical expressions, and although it is necessary to perform experimental measurements to identify the circuit parameters, the relationship between accuracy and practicality makes it the preferred to implement in the battery management systems (BMS) of the vehicles.

The BMS monitors the battery status ensuring its safety and performance [17]. It intends to keep the battery in a reliable operating area, to check its actual state and predict its capability. To perform these tasks, the BMS needs to estimate different parameters such as terminal voltage, current, temperature, open circuit voltage (OCV) and, among other states, the state of charge (SoC). The SoC is generally defined as the ratio of the remaining capacity (stored charge available to do work) to the reference capacity (the current maximum capacity the battery can release at a constant current rate and a specific ambient temperature as the manufacturer suggests). An accurate estimation of the SoC is one of the most important issues of the BMS. It provides a measure not only of the available energy and the remaining useable time of the battery, but also about its instantaneous power capability. Therefore, a real-time monitoring of SoC is crucial. Unfortunately, it cannot be directly measured but must be estimated from the measurements of other battery quantities. The non-linear time-varying characteristics and electrochemical reactions involved in the battery system and, on the other hand, the effects of aging, temperature and charge-discharge cycles make this task even especially difficult. That is why developing accurate methods for SoC prediction remains challenging in research (see, for instance, [6,18,25,21], to mention some recent works).

There is a large amount of literature about battery's SoC estimation methods. Some recent in-depth reviews can be found in [29,20,14,24], for instance.

From these reviews we deduce that equivalent circuit models (ECM)+ Kalman filter (KF) family based estimation method are the most commonly used combination as online SoC estimation techniques and, in particular, the Extended Kalman Filter (EKF) ([17,23,7,26]). The main advantage of KF based methods to estimate SoC is that it can be performed very accurately and continuously. Nevertheless, there are still different significant error sources as aging, temperature and, specially, hysteresis effects. In fact, many times the problem lies not only in searching highly accurate and strongly robust estimation but also on modelling the hysteresis cell accurately.

For a battery cell, hysteresis means that the cell reaches different OCV values at the same SoC point and temperature between charge and discharge, depending on the previous charge-discharge history. In particular, experimental results show that the OCV after discharging always relaxes to the point below the OCV after charging for the same SoC. Equivalently, for a given open circuit voltage a range of SoC may exist depending on the conditions created by historical charging and discharging cycles (see Figs. 2a and 4). As a consequence, the SoC-OCV relation is not a one-to-one mapping but a bundle of curves enclosed in the so-called major loop. This is composed of two SoC-OCV curves obtained by charging/discharging completely the battery very slowly, first to minimum voltage and then to maximum voltage while recording battery voltage and accumulated ampere hours, for one complete battery cycle. Minor loops lying inside the major loop can be obtained by conducting a similar experiment but with partial cycles. An example of hysteretic behavior experimentally measured on a 1.1 Ah LFP is given in Fig. 4.

It is well-known that hysteresis has a profound impact on the ability to monitor battery performance and this is why there are extensive studies addressing the OCV hysteresis modelling. The phenomenon can be neglected for some kind of battery types, but for LFP batteries the effects of hysteresis are very pronounced and non-ignorable [30].

A simple approach is to average the major loop and to relate the battery's OCV with its SoC through this average curve (see Fig. 6), but this approximation usually suffers from a relevant error in the real OCV estimation. On the other hand, when applying an EKF algorithm variant based on ECM containing a Coulomb counting method for SoC estimation, the error on the OCV estimation is introduced into the SoC estimator, leading to cumulative SoC errors on voltage flat regions.

Therefore, to improve the accuracy of the algorithms for SoC estimation, it is important that the ECM incorporates models capable to deal with the cell hysteresis accurately.

For this purpose, in this paper we use the classical Preisach hysteresis model, widely employed in the area of magnetism. A complete description of the model can be seen in [15]. In particular, it allows to reproduce not only the major loop boundaries but also the different minor loops. An important property of the Preisach operator is rate-independence. This characteristic fits well with the battery hysteresis behavior in the sense that it depends on the SoC history but not on the speed with which SoC is changed.

In the literature, we find some few works handling the battery hysteresis based on different approaches to this model [9,2]. A first attempt to model lithium-ion batteries hysteresis with the classical Preisach model can be found in [9]. The SoC is seen as the superposition of the SoC of elementary mathematical units having only two states: fully charged and empty and they switch from one state to the other on response to an external field. Their switching fields are distributed according to a density function, which is assumed to be an a priori known analytical function which the authors try to adapt to experimental curves. They apply the method only to the description of major loops. The authors in [2] apply the classical Preisach model for the static modelling of a fresh LFP cell SoC–OCV characteristic at fixed temperature, overcoming the intrinsic limitations and drawbacks highlighted in [9].

We adopted the classical implementation of the Preisach model described in [15,3] and which is the same adopted by [2], where the Preisach operator is discretized by means of the so-called Everett function. Compared to other models, the main advantage is that the procedure to identify the Everett function is based on experimental data depending on the battery cell technology, which avoids any heuristic approach to parameter or operator identification appearing in other models. Moreover, it is computationally appropriate for the online SoC estimation.

Two main differences of our work with respect to [2] can be highlighted. First of all, in order to make the measurements needed to build the Everett function, we propose a procedure which only involve the charging curves of the battery. Thus, a significant reduction in the time employed for laboratory experiments is achieved. We also propose a new procedure to compute the Preisach operator which avoid the need of any substantial modification of the classical model used in magnetic hysteresis. The model has been assessed with some laboratory experiments performed on a lithium-ion battery (but in fact the same procedure can be applied to other technologies) and the results show that with this procedure hysteresis is well reproduced, even when interior loops are present. Secondly, we propose to combine the hysteresis model and ECM with an Extended Kalman Filter (EKF). Using this technique, it is possible to achieve a more accurate real SoC estimation.

Up to the authors knowledge, none of the works in the literature deals at the same time with the combination of these two techniques (Preisach via Everett approximation and EKF) to estimate the SoC.

The rest of the paper is organized as follows: Section 2 recalls the first order ECM for batteries and briefly discuss the hysteresis in the SoC-OCV relationship. Then, the Preisach hysteresis model based on Everett function is described in Section 3 and the characterization of this function is done and validated via some experimental tests on an 1.1 Ah LFP battery. Section 4 deals with the electrical model verification, including the test bench in plant. In Section 5 the methodology for SoC estimation using the EKF is introduced and applied; the experimental setup and simulation results are also reported. In Section 6 the previous methodology is applied to a second order ECM. Section 7 gives some conclusions and final remarks.

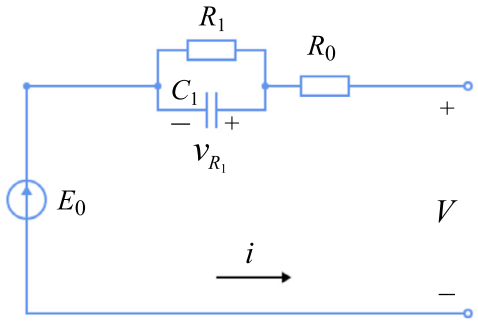

Fig. 1. A first order circuit model.

2. Equivalent circuit model and hysteresis

The battery behavior will be modelled by the circuit shown in Fig. 1. It consists basically of the so-called equivalent series resistance (ESR) (R_0) and a resistor-capacitor (R_1, C_1), the latter allows modelling the so-called diffusion voltages. In general, R_0 is a sum of resistive contributions from different elements of the battery, including the heat loss in the electrolyte. In this work it simply reduces to the ohmic resistance of the electrodes and connections. The notations employed from now on are the usual ones: Q is the maximum charge of the battery (also called total capacity or simply capacity), $i(t)$ the current intensity, $V(t)$ the voltage, $z(t)$ the state of charge (SoC) (defined as the percent of the charge stored in the battery with respect to its maximum nominal value), $\eta(t)$ the Coulombic efficiency, R_1 the polarization resistance, C_1 the polarization capacitance, and $v_{R_1}(t)$ is the voltage between the ends of the resistor R_1 (see [17] for more details about the physical meaning of these parameters).

This circuit model for the battery leads to the following problem:

Given functions $\widehat{OCV}$, $i(t)$ and $\eta(t)$, constant parameters Q, R_0, R_1 and C_1, and initial conditions z_0 and $v_{R_{1,0}}$, find functions $z(t)$, $V(t)$ and $v_{R_1}(t)$, satisfying,

$$\frac{dz}{dt}(t) = -\frac{1}{Q}\eta(t)i(t) \tag{1}$$

$$\frac{dv_{R_1}}{dt}(t) + \frac{1}{R_1C_1}v_{R_1}(t) = \frac{1}{C_1}i(t) \tag{2}$$

$$v_{R_1}(0) = v_{R_{1,0}} \tag{3}$$

$$z(0) = z_0 \tag{4}$$

$$V(t) = \widehat{OCV}(z(t)) - v_{R_1}(t) - R_0 i(t), \tag{5}$$

where function $\widehat{OCV}$ gives the OCV from the state of charge z. We consider the SoC as the independent variable, as it seems to us more easy to control SoC rather than OCV. It is known that the LFP batteries are characterized by a small variation of (an almost constant) OCV when the stored charge is in the interval between 20% and 80% of its maximum value. In addition, the function mapping OCV as a function of the SoC is not a single valued mapping but exhibits a pronounced hysteresis. As we have mentioned in the introduction, this means that OCV value varies at the same SoC point between charge and discharge. In fact, a range of SoC may exist, depending on the conditions created by historical charging and discharging cycles. In other words, values of OCV not only depend on the present values of SoC but also on the past history. To take the hysteretic behavior involved in the SoC-OCV relation into account, we will employ the classical Preisach hysteresis model which has been extensively used to characterize ferromagnetic materials [15,3].

3. Preisach hysteresis model based on Everett function

Hysteresis is a phenomenon deeply studied in magnetics and one of the most used magnetic hysteresis models is the Preisach model [15,22]. It was originally proposed by Preisach in 1935 and later formalized in a general way to take into account the similarity of hysteretic behaviors in different fields [3,4]. In particular, this model has been applied to describe LFP battery hysteresis in [2].

The classical Preisach hysteresis operator reads as follows

$$y(t) = \iint_{\rho_2 \geq \rho_1} \gamma_{\rho_1\rho_2}(u(t), \xi)\, \mu(\rho_1, \rho_2)\, \mathrm{d}\rho_1\, \mathrm{d}\rho_2, \tag{6}$$

where μ is a weight function (also called Preisach function), ξ contains the information about the initial state of battery and $\gamma_{\rho_1\rho_2}$ is the relay function depicted in Fig. 2b. It is known that SoC-OCV hysteresis loop cannot be directly modelled by the classical Preisach model and a modification is needed (see [27]). Here we propose a new approach which avoid the need of any substantial modification of the Preisach model. In fact, the only modifications with respect to (6) are the integration domain and a constant value, thus the SoC-OCV relation is modelled by:

$$OCV(t) = \widehat{OCV}(SoC, \xi)(t) = \iint_{T} \gamma_{\rho_1\rho_2}(SoC(t), \xi)\, \mu(\rho_1, \rho_2)\, \mathrm{d}\rho_1\, \mathrm{d}\rho_2 + K_{\mathrm{OCV}} \tag{7}$$

where T is a Preisach triangle (see Fig. 2f) and

$$K_{\mathrm{OCV}} = \iint_{T} \mu(\rho_1, \rho_2)\, \mathrm{d}\rho_1\, \mathrm{d}\rho_2 + OCV_{\min}$$

where $OCV_{\min}$ is the minimum OCV value. Notice that $\widehat{OCV}(0) = OCV_{\min}$ (see Fig. 2a). To compute the hysteretic term of (7) we proceed as in [15] and decompose the Preisach triangle into two sets: S^+ and S^-, such that the relays are $+1$ in S^+ and -1 in S^- (see Fig. 2c- 2d). Thus we get

$$OCV(t) = \iint_{S^+} \mu(\rho_1, \rho_2)\, \mathrm{d}\rho_1\, \mathrm{d}\rho_2 + OCV_{\min}. \tag{8}$$

In the same reference, an approach is developed for the computation of the Preisach model that does not require the Preisach function μ that identifies the battery but the so-called Everett function which describes the effect of μ on the hysteresis operator. Let us notice that the formalism of the Everett function for the classical Preisach modelling is the same. This is due to the fact that we have only added a constant value to the classical model representation (see (7)). To obtain the Everett function, the so-called first order reversal curves (FORC) are required (see Fig. 2e). A FORC diagram is generated from a class of minor hysteresis loops referred to as first-order reversal curves. The acquisition of a FORC begins by saturating a system. The applied field is lowered to a reversal field, and a FORC is the curve that results when the field is increased back to saturation. Let us consider an example to illustrate the relation between the FORC, the Everett function and the Preisach model. We consider a function u representing the SoC, such that at time t_0 the battery is fully charged at its nominal capacity, i.e., $u(t_0) = 100\%$. Then, u decreases monotonically until it reaches some value ρ_1' at time t_1 (see Fig. 2e). We denote $w_{\rho_1'} := OCV(t_1)$. A first order reversal curve is formed by the above monotonic decrease of u followed by a subsequent monotonic increase, namely, from ρ_2', u increases monotonically until it reaches some value $\rho_1' < \rho_2'$ at time t_2; we denote $w_{\rho_2',\rho_1'} := OCV(t_2)$ (see Fig. 2e). We define the Everett function E by

$$E(\rho_1', \rho_2') := \frac{w_{\rho_2',\rho_1'} - w_{\rho_1'}}{2}. \tag{9}$$

It can be shown the following relation between the Preisach density function μ and the Everett function E:

$$E(\rho_1, \rho_2) = \int_{T(\rho_1,\rho_2)} \mu(\rho)\, d\rho \qquad \forall (\rho_1, \rho_2) \in T \tag{10}$$

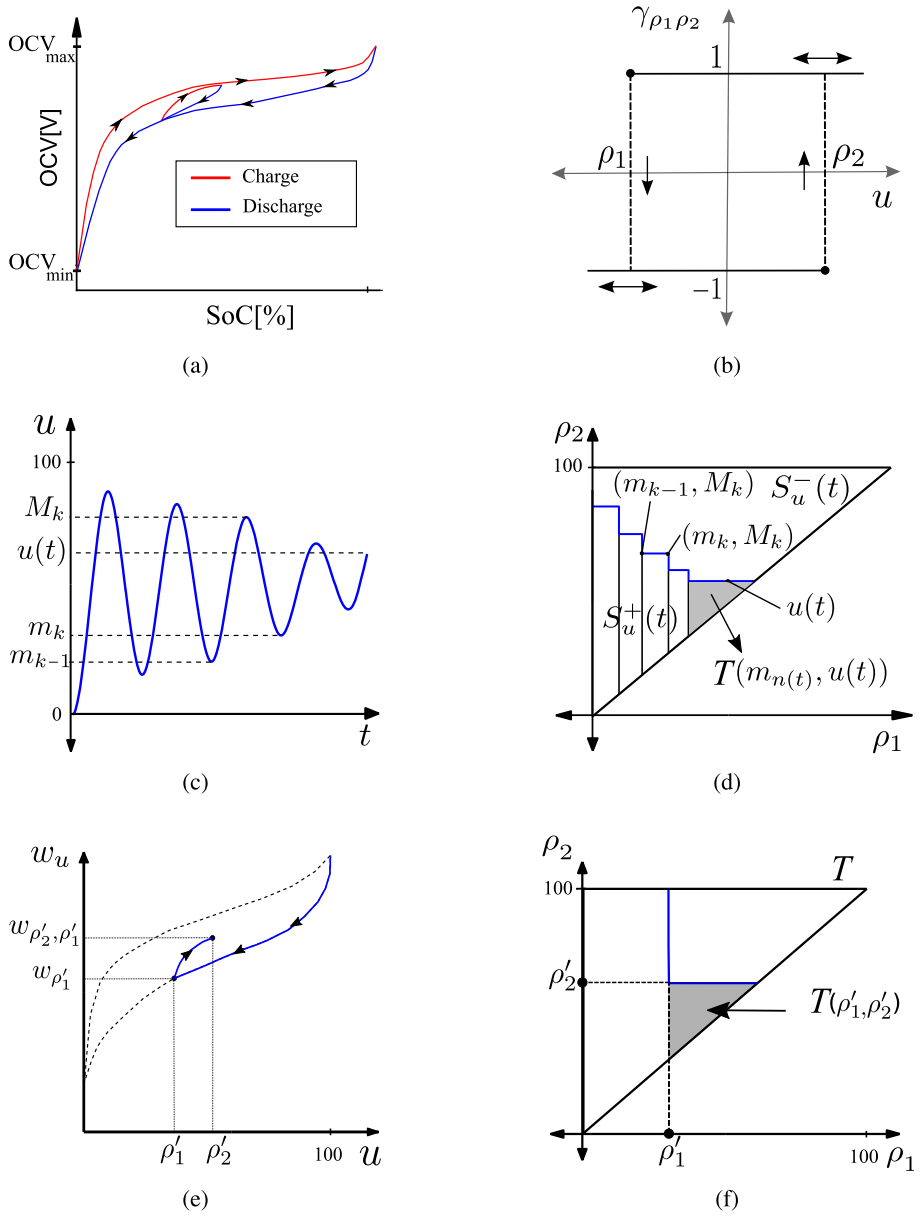

Fig. 2. (a) Hysteresis loop SoC versus OCV. $OCV_{\min}$ and $OCV_{\max}$ represent the maximum and minimum values of OCV, respectively. (b) Relay. (c) Input signal u and (d) corresponding decomposition of the Preisach triangle $T = S_u^+ \cup S_u^-$. (e) First order reversal curve and (f) Preisach triangle.

with $T(\rho_1', \rho_2')$ being the triangle shown in Fig. 2f with the vertex of the right angle at (ρ_1', ρ_2'). Using the previous equality, (8) can be rewritten as (see [15]):

$$OCV(t) = 2\sum_{k=1}^{n(t)} \left(E(m_{k-1}, M_k) - E(m_k, M_k)\right) + OCV_{\min}, \tag{11}$$

where $n(t)$ is the number of local maxima of SoC up to time t that have not been wiped-out and M_k and m_k are the local maximum and the local minima, respectively (see Fig. 2d). The wiping-out property of hysteresis means that only dominant extreme values are stored in the Preisach model and all the other input local extreme values are wiped out.

3.1. Characterization of the Everett function

In this section we consider an experimental setting based on the major loop and FORC branches to reconstruct the Everett function which, as stated before, identifies the Preisach hysteresis model. All the tests are run at XCTS BaSyTec test benches placed on an ambient temperature controlled room set at 25 °C. We have tested three fresh cells of the same batch and select randomly one of them after checking that the obtained results are reproducible. The characteristics are detailed in Table 1. The OCV values of the mayor loop and these FORC branches are measured based on three types of tests: a capacity characterization test, a pulse test and a relaxation test.

Table 1
Cell APR18650M1A characteristics.

Chemistry	LFP
Nominal voltage	3.3 V
Charge cutoff voltage	3.6 V
Discharge cutoff voltage	2 V
Nominal capacity	1.1 Ah
Maximum discharge current	30 A
Maximum charge current	4 A
Operating temperature range	[−30 °C +60 °C]

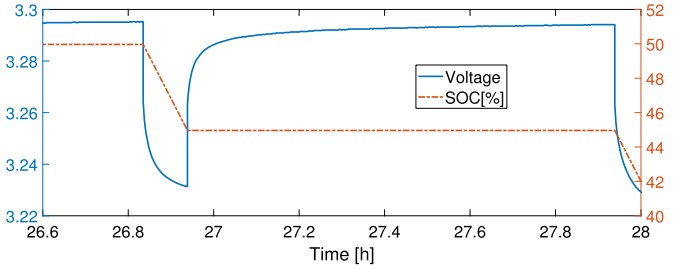

Fig. 3. Battery SoC and voltage during one cycle.

- Firstly, a capacity characterization test based on the standard IEC 62660-1 is run [11]. We have applied two Constant Current-Constant Voltage (CC-CV) charges and two CC discharges at the nominal current rate. The current threshold for the CV phase is set to 5% of the nominal charge current. The dischargeable capacity measurement is done at the end of the second discharge.
- Secondly, pulse tests at the nominal current rate are applied with which the SoC level of the battery is modified. Thanks to the already measured dischargeable capacity, we are able to define the amount of Ah that need to be charged and discharged in each pulse to change the SoC to the desired value. We have observed that we are able to reach the desired SoC value with an error below 0.1%.
- Thirdly, a relaxation of 1 h is applied on each SoC of interest so as to establish the battery inner reactions. The measured voltage at the end of the 1 h rest period is considered to be the OCV [13] (see Fig. 3).

The initial capacity characterization test along the combination of pulse tests and relaxation tests according to the defined FORC branches give as a result the SoC-OCV measurements required in the Everett function (Fig. 4). Our testing proposal differs slightly from the one proposed in [2] and requires 212 less relaxation periods. This results in 212 hours experimentation time saving, which is a significant reduction. Besides, our proposal is measuring the FORC branches with a 2% SoC difference, while the proposal in [2] has a SoC step of 5%.

Since the experiments are defined on a coarse discretization of the Preisach triangle T, the Everett function has been reconstructed on a more fine and regular mesh. This procedure was done first, by a one-dimensional (1D) interpolation of each FORC branch and then, another 1D interpolation in the orthogonal direction. Both interpolation were performed with MATLAB command *pchip* which preserve the monotonic behavior of the data. A two-dimensional (2D) representation of the Everett function defined on a fine mesh is depicted in Fig. 5.

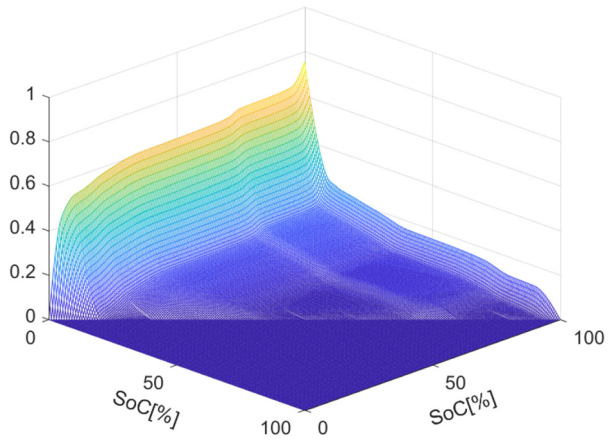

Fig. 5. Everett function.

We recall that the Everett function identifies the Preisach model for the LFP battery studied in this work; thus, the previous Everett function can be used to compute (11) for any input value by means of 2D piecewise linear interpolation.

3.2. Validation

We compare the SoC-OCV curves from experimental data with the curves computed with the Preisach model identified by the Everett function described before. The approximations are reported in Fig. 6 where the values simulated with the Preisach model are plotted together with the experimental results. We have also included the average open circuit voltage OCV_{av} defined by:

$$OCV_{av}(SoC) = \frac{OCV_{up}(SoC) + OCV_{lw}(SoC)}{2} \tag{12}$$

where $OCV_{up}(SoC)$ and $OCV_{lw}(SoC)$ are the upper and lower bounds of the major hysteresis loop, respectively. These functions are computed by interpolating experimental data. The major loop is well approximated by the hysteresis model, in particular those SoC values between 10% and 90%. The relative error of the major loop is 0.021% and there is not a significant difference between the relative errors on the fully charge/discharge region and the region where the SoC varies within 10% and 90%. In order to test the approximation properties of the hysteresis model, we have considered measurements for inner loops that were performed in a different cell from the one we obtain the FORC branches. Minor loops bounded between SoC values of 10% – 40%,

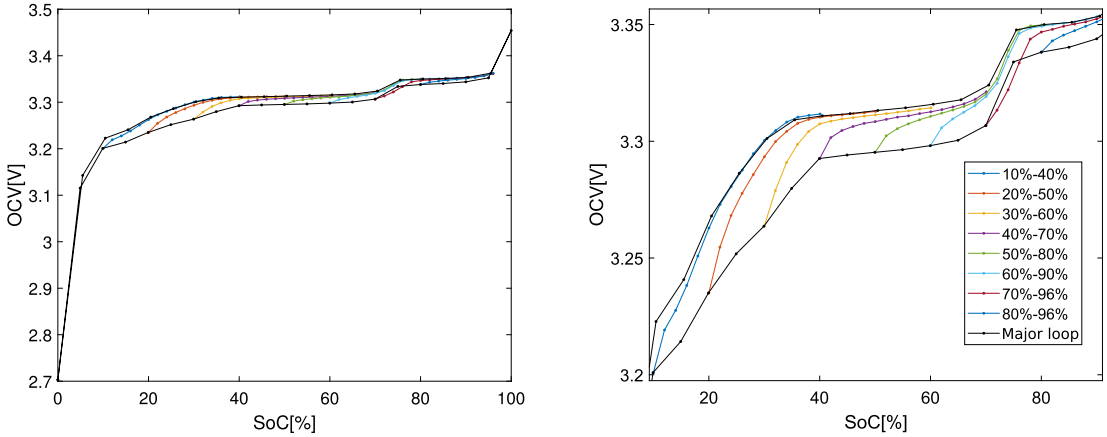

Fig. 4. SoC-OCV measurements for major loop data and eight charge inner branches (left); zoom 10%-90% (right).

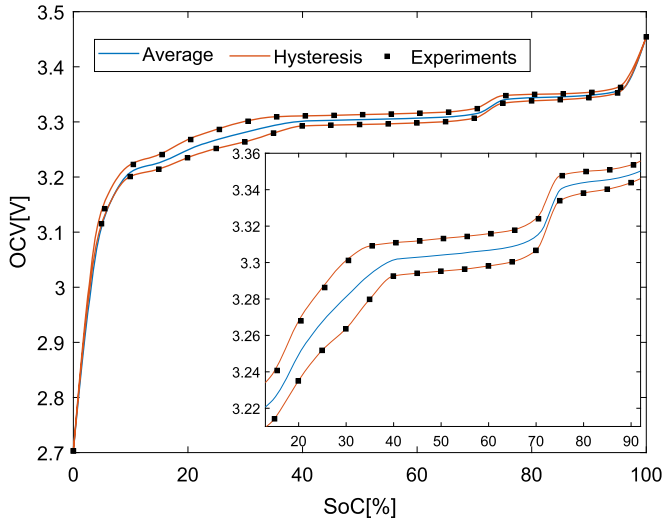

Fig. 6. Measurements along the major loop and the approximation given by the Preisach model and average OCV.

25% – 55%, 35% – 65% and 40% – 70% are depicted in Fig. 7a-7d. The relative errors of the minor loops are 0.096%, 0.184%, 0.071% and 0.044%, respectively. Notice that, although only the charge branches were used to identify the Preisach model, discharge branches are very well approximated. From the previous results it can be seen that the SoC-OCV hysteresis behavior of the battery can be predicted by the Preisach model constructed from ascending FORC curves. The errors in the approximation of the major loop and inner loops in the SoC interval 10% – 70% are small.

4. Electrical model verification

First of all, the equations for the equivalent circuit shown in Fig. 1 and a Coulomb counting method are developed in the discrete space state form. Discrete-time model assumes that the cell inputs and outputs are measured at a regular rate with period Δt seconds. Superscript k denotes the value of the discrete time sample at instant "$k\Delta t$". Then, (1) and (2) are discretized by using a finite difference scheme relating the sample values z^k and $v_{R_1}^k$ (see, for instance, [17, Section 5.1.2]). The discrete model reads as follows:

$$\begin{pmatrix} z^{k+1} \\ v_{R_1}^{k+1} \end{pmatrix} = \begin{pmatrix} 1 & 0 \\ 0 & e^{-\frac{\Delta t}{R_1 C_1}} \end{pmatrix} \begin{pmatrix} z^k \\ v_{R_1}^k \end{pmatrix} + \begin{pmatrix} -\frac{\Delta t \eta}{Q} \\ R_1 (1 - e^{-\frac{\Delta t}{R_1 C_1}}) \end{pmatrix} i^k \tag{13}$$

$$V_k = \widehat{OCV}(z^0, z^1, \ldots, z^{k+1}) - v_{R_1}^{k+1} - R_0 i^k. \tag{14}$$

Vector $x^k = (z^k, v_{R_1}^k)$ is the system state-vector at time index k and contains the SoC estimator, the voltage across the R_1C_1 network and the voltage drop in the Ohmic resistance R_0. The output of the system is V_k given by (14). Each measurement interval, the model updates its state and output values based on its input. To describe the dynamic evolution of the SoC, the Coulomb counting equation has been used considering the nominal capacity of the cell (Q) and the simulation time step (Δt). The fitting of each parameter of the ECM (R_0, R_1 and C_1) has been done using least square technique and are depicted in Fig. 8a.

We have considered a realistic light duty vehicle driving profile to quantify the accuracy of the ECM with hysteresis: the Highway Fuel Economy Cycle (HWFET). This driving profile has been converted into a current profile and scaled to the characteristics of the selected battery (to a maximum charge current of 4 A and to a maximum discharge current of 30 A). The obtained current profile has been applied repeatedly on the middle flat part of the operation window: from 3.6 V to 3 V. The HWFET current profile has been repeated 5 times on this voltage range.

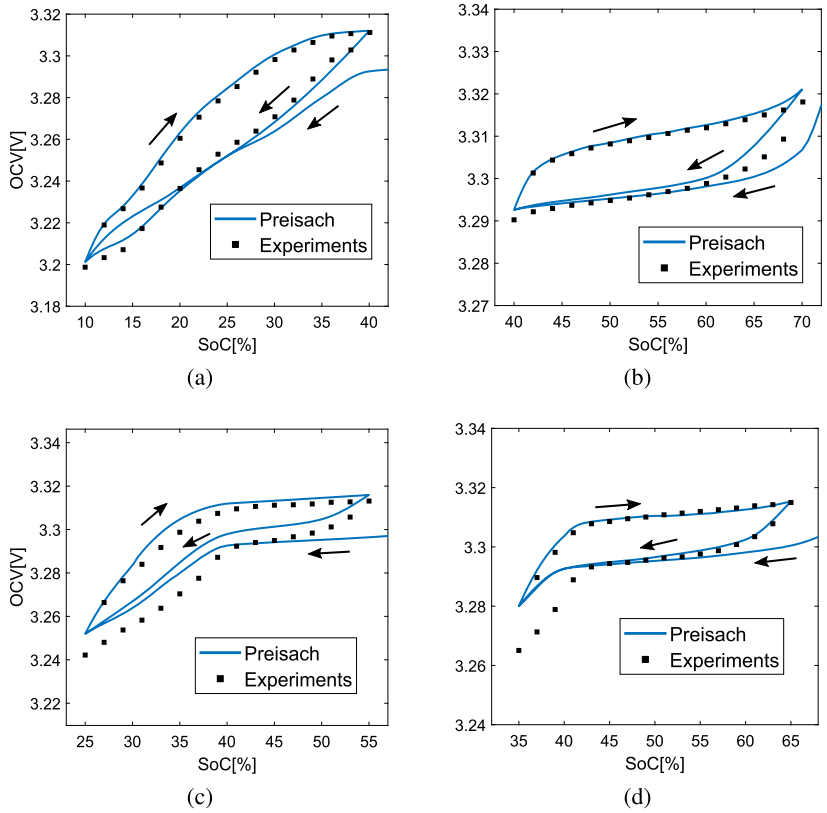

Fig. 7. Experimental inner loop and approximation of the Preisach model for different SoC values. From top to bottom: 10%-40%, 40%-70%, 25%-55%, 35%-65%.

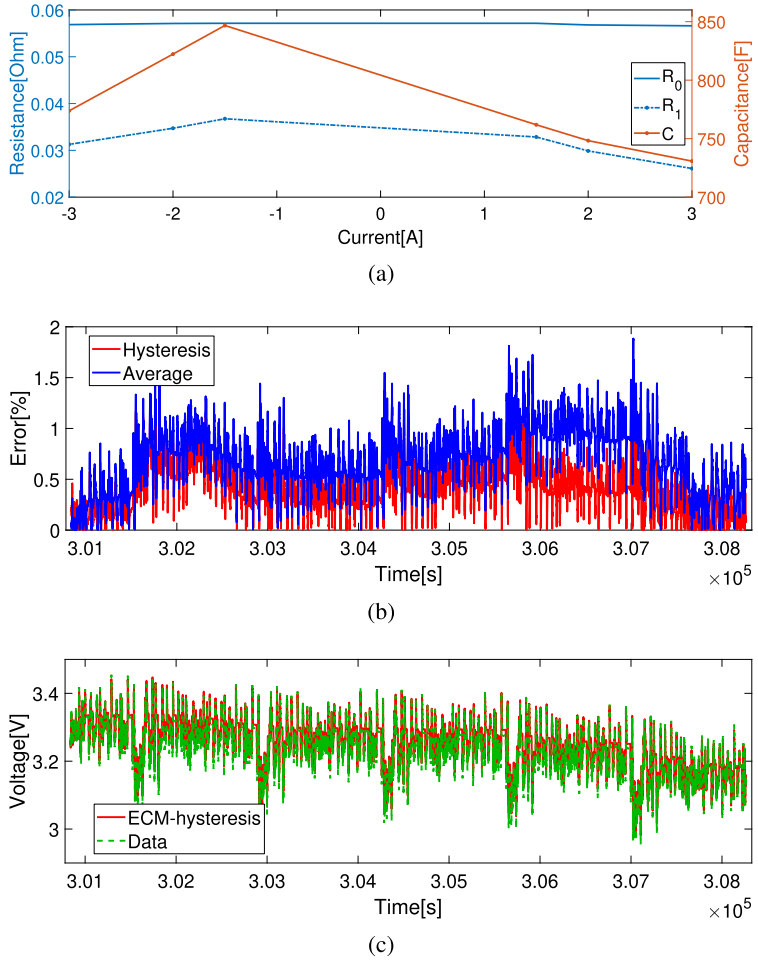

Fig. 8. (a) Evolution of R_0, R_1 and C_1 at 50% SoC. (b) Percentage error in the voltage approximation (c) Measured and computed voltage with ECM and Preisach model.

As a result, the response of the battery in the region more significantly affected by hysteresis is observed and used in the validation.

We have solved (13) and compared the computed voltage (14) with the experimental value. The values of OCV are computed with the average open circuit voltage curve (12) and with the Preisach hysteresis model (cf. (7)) with Everett function characterized in the previous section and depicted in Fig. 5. Fig. 8b shows the error between the experimental voltage and the voltage computed with OCV_{av} and the Preisach model. It can be seen that the error is smaller when the Preisach model is considered. The comparison between the measurement and the estimated value of the voltage is shown in Fig. 8c. The result has been excellent, having a relative error of 0.401%.

From the previous analysis, we conclude that the proposed ECM with hysteresis combined with the above described experimental methodology to identify the hysteresis operator yield a good approximation of the behavior of the battery and thus can be considered for the SoC estimation studied in the next section.

5. Extended Kalman filter

As mentioned in the introduction, during the last years several methods have been proposed for estimating the SoC: Coulomb counting, discharge test, open circuit voltage measurement, impedance spectroscopy, linear equivalent methods, neural networks, fuzzy logic, stochastic filters, among others (see, for instance, [10,29,1]). However, most of them present some disadvantages such as measurements accuracy, long rest periods dependency, technical complexity or the necessity to perform long training tests. In this sense, stochastic filters, are very good alternative due to the state updating by means of the comparison between estimated and measured results.

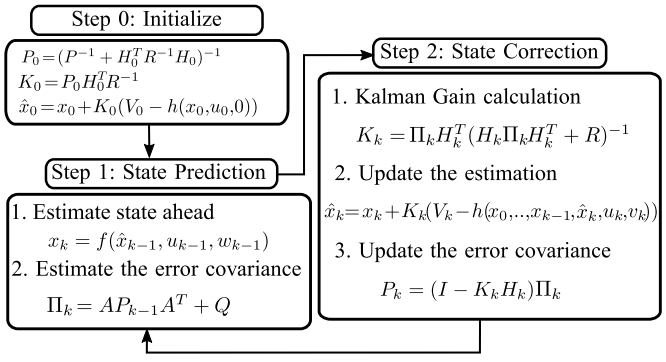

Fig. 9. Sketch of the EKF algorithm.

In this work we apply the EKF [17] which estimates recursively the unknown state of nonlinear systems by solving the model equations and using measurements. This procedure consists of three steps (see Fig. 9):

- Initialization: a-priori state-vector (x_0) and the covariance matrix of its corresponding random error (P_0) are initialized.
- State prediction: a priori estimates of the state vector x_k and the covariance matrix Π_k are performed considering the ECM and the covariance propagation equation.

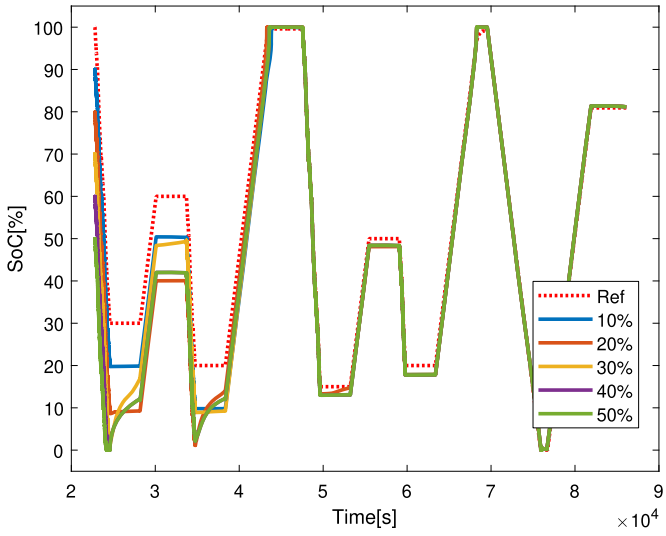

Fig. 10. EKF SoC estimations for different initial conditions.

- State correction: Kalman gain (K_k) is calculated first and then it is used to compute the a posteriori state estimation $\hat{x}_k$. This correction is done according to the measured voltage (V_k) and the estimated voltage from the ECM and the $\widehat{OCV}$. Similarly, a posteriori estimation, P_k, of the covariance matrix is calculated.

Here, $x_k = (z^k, v^k_{R_1})$, $u_k = i^k$ and the linear and non linear functions f and h are given by (13) and (14), respectively. Given the history dependence of the hysteresis operator, we notice that h at stage k, depends on $x_0, x_1, \ldots, x_k$, namely, $h = h(x_0, x_1, \ldots, x_{k-1}, u_k, w_k)$. On the other hand, the process noises w^k and the measurement noises v^k are independent Gaussian random vectors with zero mean and covariance matrix Q and R, respectively. For being applicable the Kalman filter theory to non linear systems, the EKF calculates the first derivatives of the state and output equations

$$A([i,j]) = \frac{d(f(x_{k-1}, u_k, w_k)_{[i]})}{dx_{[j]}},$$

$$H_k([i,j]) = \frac{d(h(x_0, x_1, \ldots, x_k, u_k, w_k)_{[i]})}{dx_{[j]}}.$$

We notice that A is constant along the time and it is easily computed as the state equation is linear. However, H_k changes along the time and it is computed numerically. We also notice that, in order to compute the derivative of OCV respect to SoC at step k, the values of SoC at steps $0, \ldots, k-1$ are used.

Next, the performance of the filter is quantified. For this purpose, data of a test staying at intermediate SoC is used. The test consists of two steps: firstly, the capacity characterization test used in the FORC branches estimate; secondly, a combination of CC charges at nominal current rate and repeated HWFET discharges, where the charge and discharge are cutoff based on some SoC predefined values: 100%-30%-60%-20%-100%-15%-50%-20%-100%-0%-80%, is applied to the battery. The same tests have been made but using a *wrong* initialization, namely, 10%, 20%, 30%, 40% and 50% SoC error) aiming to observe the convergence of the estimated SoC to the SoC reference which has been calculated by the Coulomb counting method due to the excellent measurement accuracy of the equipment used in this work (0.05%).

It can be seen in Fig. 10 that all the wrong initial values are corrected along the time: the EKF estimates reduce the initial error and converge to the reference SoC. The error is particularly reduced at the end of charging processes where the observability degree of the SoC is increased and, as a consequence, the EKF is able to correct the estimation. For this test, the covariance matrices are chosen as follows: P and Q are diagonal matrices with entries [50 5] and [100 5], respectively and $R = 10^{-6}$.

Fig. 11 shows the voltage predicted by the model, the measured voltage and the voltage given by the Kalman filter corresponding to a *wrong* initial condition with 50% error in the SoC. Notice the superposition of the curves corresponding to the Kalman filter and that corresponding to the experimental measurements.

To conclude this section, and for the sake of completeness, we have compared the classical 1RC model with the improved one, considering the EKF in both cases (initial condition with 10% error in the initial SoC is taken). The results in Figs. 12a and 12b show that the improved 1RC model plus the filter performs better than the classical one with the filter.

6. Extension to a 2RC model

The method detailed in the previous sections for a 1RC circuit model can be extended to a general n-th order RC model. In this section we show the results obtained for a second order circuit model (2RC) with averaged parameter values $C_1 = 7.3800 \times 10^2$ F, $R_1 = 0.01629$ Ohm, $C_2 = 2.2522 \times 10^5$ F, $R_2 = 0.5479$ Ohm, $R_0 = 0.0547$ Ohm. To begin with, and in order to carry out an analysis similar to that of the previous sections, we have compared the classical 2RC model (i.e., when considering the averaged curve of the SoC-OCV major loop) with the improved 2RC one (i.e., considering the hysteresis) and without applying any filter, namely, when input values of Section 4 are considered. Fig. 13 shows the percentage voltage error obtained when comparing these two models. As expected, when hysteresis is considered the model performs better. Moreover, as it can be deduced from Fig. 14, the second order model is preferable.

Next, we compare the second order models (classical versus improved one) when the EKF is considered. With this aim we proceed as in Section 5. In this case, the covariance matrices are chosen following the methodology explained in [5]. In particular, and following the notation in [5], the diagonal matrix $P_0 = [50\ 5\ 5]$, $\delta = 10^{-1}$, $\gamma = 10^8$ and $\lambda = 10^{-12}$. The results presented in Fig. 15 show that the EKF applied to the improved 2RC model produces better results than when applied to the traditional 2RC model.

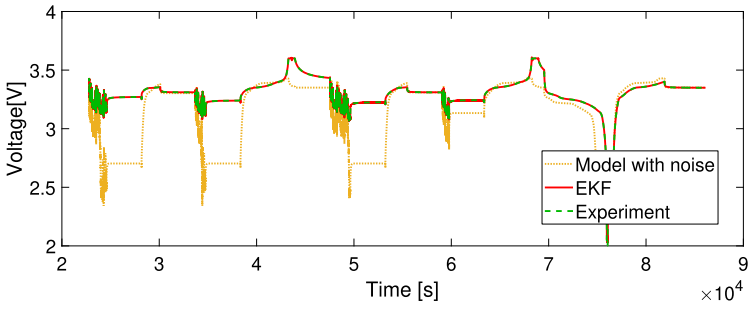

Fig. 11. Comparison of the voltage obtained with different methods. Initial condition with 50% error in the initial SoC.

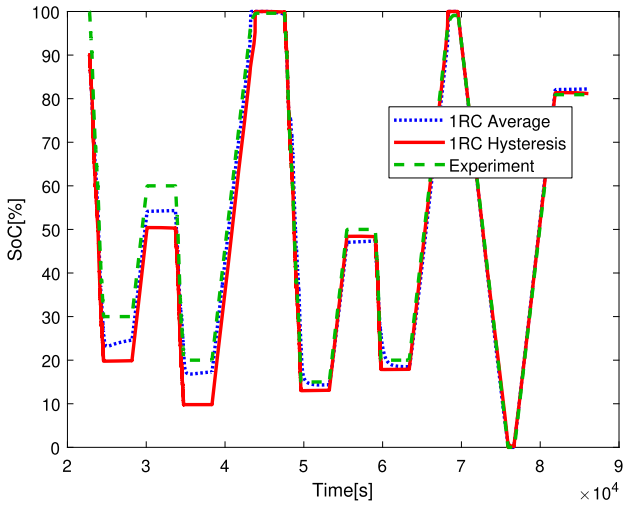

(a)

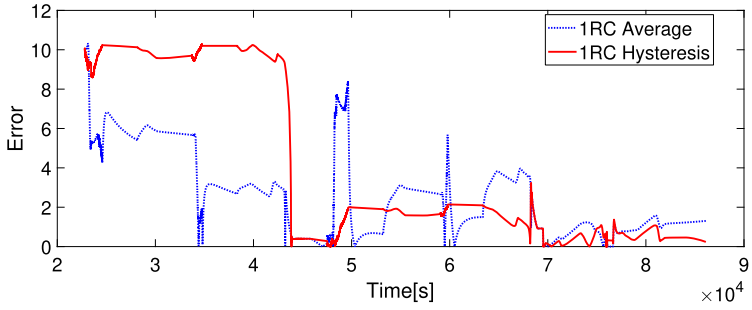

(b)

Fig. 12. Classical 1RC model versus improved 1RC model. (a) SoC approximation (b) Absolute error.

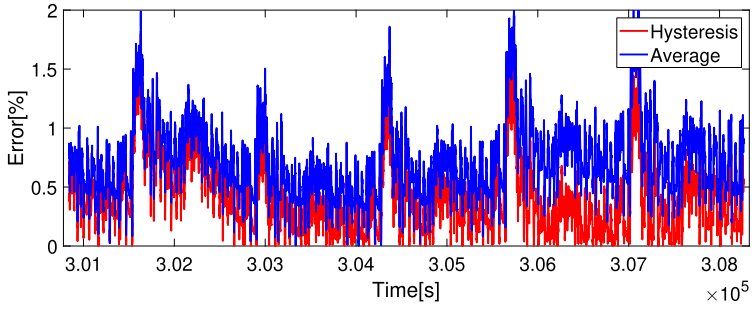

Fig. 13. Percentage voltage error. Classical versus improved 2RC model.

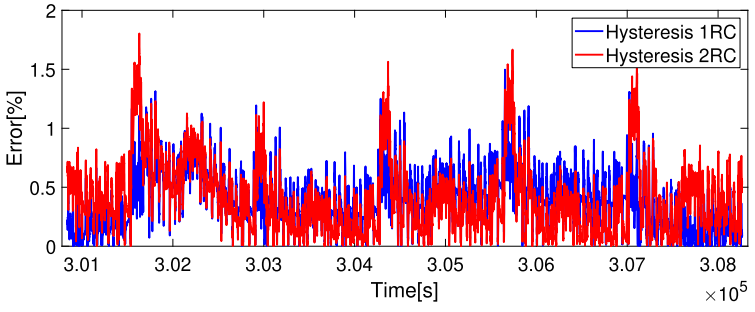

Fig. 14. Percentage voltage error. 1RC versus 2RC improved models.

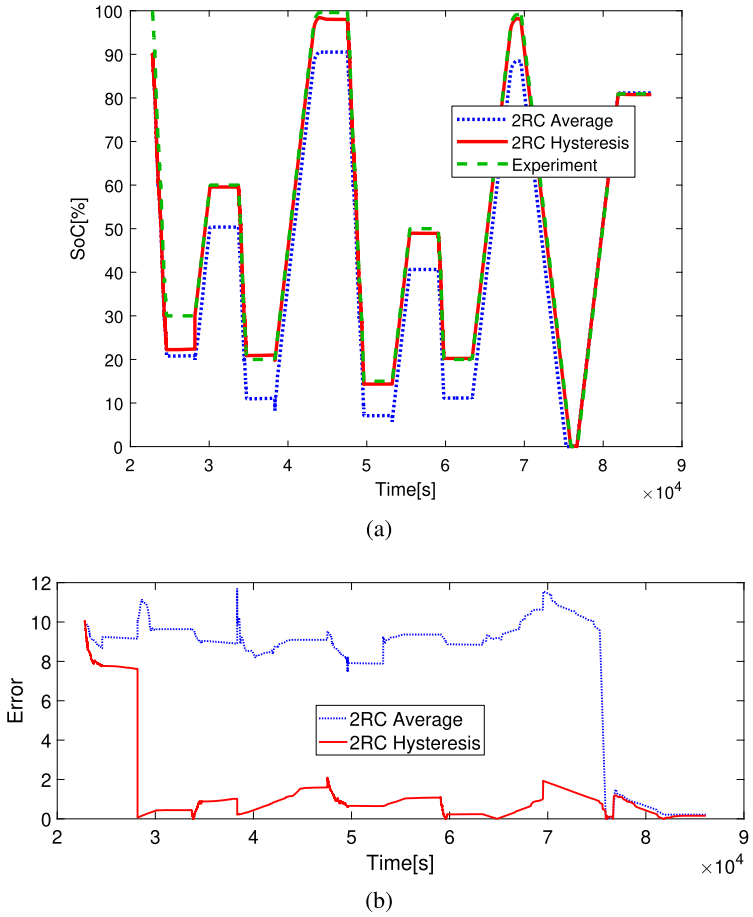

Fig. 15. Classical 2RC model versus 2RC improved model. (a) SoC approximation (b) Absolute error.

7. Conclusions

In this paper a new accurate SoC estimation has been proposed which take into account the hysteresis phenomenon. First, an equivalent circuit model where the SoC-OCV relation is modelled by the classical Preisach model, is introduced. A new approach, which avoids the need of any substantial modification of the Preisach model, is presented.

The hysteresis operator is identified by means of the Everett function, which is obtained through experiments. A procedure based on FORC curves which significantly reduces the amount of time devoted to experimental measurements is proposed. We compare SoC-OCV experimental loops with those computed by the Preisach model for different SoC histories. The model accurately approximates measurements, both for the major loop and for minor loops. The ECM with hysteresis is validated under variable current pulses exciting the battery, showing that the model correctly reproduces the voltage. Finally, an EKF applied to the ECM with hysteresis is proposed. Its estimation has been validated under HWFET current profile starting from SoC initial errors and converging to the reference value. The method has been applied first to a 1RC model, but it can be extended to an n-th order RC model. In particular, it has been applied to a 2RC model and the results show a very good behavior.

Acknowledgements

This work has been partially supported by FEDER, Ministerio de Economía, Industria y Competitividad-AEI research project MTM2017-86459-R, by Xunta de Galicia (Spain) research project GI-1563 ED431C 2021/15, by DIUBB through project 2120173 GI/C and by ANID-Chile through FONDECYT grant 1211030 and Centro de Modelamiento Matemático (CMM), ACE210010 and FB210005, BASAL funds for centers of excellence from ANID-Chile.

References

[1] M.U. Ali, A. Zafar, S.H. Nengroo, S. Hussain, M. Junaid Alvi, H.J. Kim, Towards a smarter battery management system for electric vehicle applications: a critical review of lithium-ion battery state of charge estimation, Energies 12 (3) (2019).
[2] F. Baronti, N. Femia, R. Saletti, C. Visone, W. Zamboni, Preisach modelling of lithium-iron-phosphate battery hysteresis, J. Energy Storage 4 (2015) 51–61.
[3] A. Bermúdez, L. Dupré, D. Gómez, P. Venegas, Electromagnetic computations with Preisach hysteresis model, Finite Elem. Anal. Des. 126 (2017) 65–74.
[4] A. Bermúdez, D. Gómez, R. Rodríguez, P. Venegas, Mathematical analysis and numerical solution of axisymmetric eddy-current problems with Preisach hysteresis model, Rend. Semin. Mat. (Torino) 72 (1-2) (2014) 73–117.
[5] M. Boutayeb, D. Aubry, A strong tracking extended Kalman observer for nonlinear discrete-time systems, IEEE Trans. Autom. Control 44 (8) (1999) 1550–1556.
[6] C. Chen, R. Xiong, R. Yang, W. Shen, F. Sun, State-of-charge estimation of lithium-ion battery using an improved neural network model and extended Kalman filter, J. Clean. Prod. 234 (2019) 1153–1164.
[7] Z. Chen, L. Yang, X. Zhao, Y. Wang, Z. He, Online state of charge estimation of Li-ion battery based on an improved unscented Kalman filter approach, Appl. Math. Model. 70 (2019) 532–544.
[8] J. Du, F. Li, J. Li, X. Wu, Z. Song, Y. Zou, M. Ouyang, Evaluating the technological evolution of battery electric buses: China as a case, Energy 176 (2019) 309–319.
[9] V. Franzitta, A. Viola, M. Trapanese, Description of hysteresis in lithium battery by classical Preisach model, Adv. Mater. Res. 622–623 (2013) 1099–1103.
[10] M.A. Hannan, M.S.H. Lipu, A. Hussain, A. Mohamed, A review of lithium-ion battery state of charge estimation and management system in electric vehicle applications: challenges and recommendations, Renew. Sustain. Energy Rev. 78 (2017) 834–854.
[11] IEC62660-1:2018RLV. Secondary lithium-ion cells for the propulsion of electric road vehicles – part 1: performance testing, in: Standard TC21, International Electrotechnical Commission, Switzerland, 2018.
[12] W. Ke, S. Zhang, X. He, Y. Wu, J. Hao, Well-to-wheels energy consumption and emissions of electric vehicles: mid-term implications from real-world features and air pollution control progress, Appl. Energy 188 (2017) 367–377.

[13] A. Li, S. Pelissier, P. Venet, P. Gyan, Fast characterization method for modeling battery relaxation voltage, Batteries 2 (2) (2016).
[14] M.S.H. Lipu, M.A. Hannan, A. Hussain, A. Ayob, M.H.M. Saad, T.F. Karim, D.N.T. How, Data-driven state of charge estimation of lithium-ion batteries: algorithms, implementation factors, limitations and future trends, J. Clean. Prod. 277 (2020) 124110.
[15] I.D. Mayergoyz, Mathematical Models of Hysteresis, Springer, New York, 1991.
[16] S. Nejad, D.T. Gladwin, D.A. Stone, A systematic review of lumped-parameter equivalent circuit models for real-time estimation of lithium-ion battery states, J. Power Sources 316 (2016) 183–196.
[17] G.L. Plett, Battery Management Systems: Volume 1, Battery Modeling, Artech House, Boston, 2015.
[18] H. Popp, M. Koller, M. Jahn, A. Bergmann, Mechanical methods for state determination of lithium-ion secondary batteries: a review, J. Energy Storage 32 (2020) 101859.
[19] A. Seaman, T.S. Dao, J. McPhee, A survey of mathematics-based equivalent-circuit and electrochemical battery models for hybrid and electric vehicle simulation, J. Power Sources 256 (2014) 410–423.
[20] P. Shrivastava, T.K. Soon, M.Y.I.B. Idris, S. Mekhilef, Overview of model-based online state-of-charge estimation using Kalman filter family for lithium-ion batteries, Renew. Sustain. Energy Rev. 113 (2019) 109233.
[21] J. Tian, R. Xiong, W. Shen, J. Lu, State-of-charge estimation of LiFePO4 batteries in electric vehicles: a deep-learning enabled approach, Appl. Energy 291 (2021) 116812.
[22] A. Visintin, Differential Models of Hysteresis, Springer, Berlin, 1994.
[23] S. Wang, C. Fernandez, W. Cao, C. Zou, C. Yu, X. Li, An adaptive working state iterative calculation method of the power battery by using the improved Kalman filtering algorithm and considering the relaxation effect, J. Power Sources 428 (2019) 67–75.
[24] Y. Wang, J. Tian, Z. Sun, L. Wang, R. Xu, M. Li, Z. Chen, A comprehensive review of battery modeling and state estimation approaches for advanced battery management systems, Renew. Sustain. Energy Rev. 131 (2020) 110015.
[25] Z. Wei, G. Dong, X. Zhang, J. Pou, Z. Quan, H. He, Noise-immune model identification and state-of-charge estimation for lithium-ion battery using bilinear parameterization, IEEE Trans. Ind. Electron. 68 (1) (2021) 312–323.
[26] Y. Xu, M. Hu, A. Zhou, Y. Li, S. Li, C. Fu, C. Gong, State of charge estimation for lithium-ion batteries based on adaptive dual Kalman filter, Appl. Math. Model. 77 (2020) 1255–1272.
[27] W. Zamboni, C. Visone, Loop orientation and Preisach modeling in hysteresis systems, in: 2015 IEEE International Magnetics Conference (INTERMAG), May 2015, pp. 1–1.
[28] X. Zhang, H. Peng, H. Wang, M. Ouyang, Hybrid lithium iron phosphate battery and lithium titanate battery systems for electric buses, IEEE Trans. Veh. Technol. 67 (2) (2018) 956–965.
[29] Y. Zheng, M. Ouyang, X. Han, L.G. Lu, J. Li, Investigating the error sources of the online state of charge estimation methods for lithium-ion batteries in electric vehicles, J. Power Sources 377 (2018) 161–188.
[30] L. Zhu, Z. Sun, H. Dai, X. Wei, A novel modeling methodology of open circuit voltage hysteresis for LiFePO4 batteries based on an adaptive discrete Preisach model, Appl. Energy 155 (2015) 91–109.